INSTITUTE OF PHYSICS PUBLISHING SEMICONDUCTOR SCIENCE AND TECHNOLOGY

Semicond. Sci. Technol. **16** (2001) 331–338 www.iop.org/Journals/ss PII: S0268-1242(01)18060-0

Device model for quantum dot infrared photodetectors and their dark-current characteristics

V Ryzhii[1], I Khmyrova[1], V Pipa[2], V Mitin[2] and M Willander[3]

[1] Computer Solid State Physics Laboratory, University of Aizu, Aizu-Wakamatsu 965-8580, Japan

[2] Department of Electrical and Computer Engineering, Wayne State University, Detroit 48202, MI, USA

[3] Department of Microelectronics and Nanoscience, Chalmers University of Technology and Gothenburg University, Gothenburg S-412 96, Sweden

E-mail: v-ryzhii@u-aizu.ac.jp

Received 17 October 2000, accepted for publication 20 February 2001

Abstract

We propose a device model for quantum dot infrared photodetectors (QDIPs) with relatively large lateral spacing between QDs as occurs in QDIPs fabricated and experimentally investigated recently. The developed model accounts for the self-consistent potential distribution and features of the electron capture and transport in realistic QDIPs in dark conditions. The model is used for the calculation of the dark current as a function of the structural parameters, applied voltage and temperature. It explains a rather sharp increase in the dark current with increasing applied voltage and its strong sensitivity to the density of QDs and the doping level of the active region. The calculated dependences are in good agreement with available experimental data. The obtained characteristics of QDIPs are compared to those of QWIPs with similar parameters.

1. Introduction

Quantum dot infrared photodetectors (QDIPs) utilizing intersubband transitions proposed and analysed theoretically a few years ago [1] have since been extensively studied experimentally [2–10]. In particular, different InAs/GaAs, InGaAs/GaAs, InGaAs/InGaP and SiGe/Si QDIPs have been fabricated and measured. Although QDIPs are expected to exhibit several potential advantages over quantum well infrared photodetectors [1], most of the investigated QDIPs have worse characteristics than QWIPs with similar parameters [11, 12]. This pertains to the dark current and the responsivity of QDIPs. The prediction of rather high performance of QDIPs [1] was, in particular, based on the device model that assumes that QDs form dense QD layers (arrays) in which the lateral distribution of the potential is nearly uniform. In such ideal QDIPs, the QDs being small and lightly coupled preserve their sensitivity to normally incident infrared radiation (see, e.g., [13]) and low capture probability simultaneously maintaining more or less uniform in-plane distribution of the captured electrons. However, the QDIPs investigated in the recent experiments comprise relatively large QDs placed fairly far from each other. As a result, even substantially charged QD layers do not form the planar potential barriers which could effectively control the transverse electron transport through them (as in QWIPs with thermionic injection [14, 15]). This is due to the existence of 'punctures' in such potential barriers located between the QDs. Hence, the main stream of electrons injected from the emitter contact passes through these holes resulting in elevated dark current.

In this paper, we develop a device model which accounts for the features of the realistic QDIPs associated with the distinctive properties of the electron capture into QD and the electron transport through the punctures in the planar potential barriers formed by the charged QDs. The model is applied to calculate the QDIP characteristics in dark conditions, focusing on the effects of the strong dependence of the dark current on the applied voltage, density of QDs and doping. We also compare the calculated characteristics of the realistic QDIPs with those of QWIPs with similar parameters.

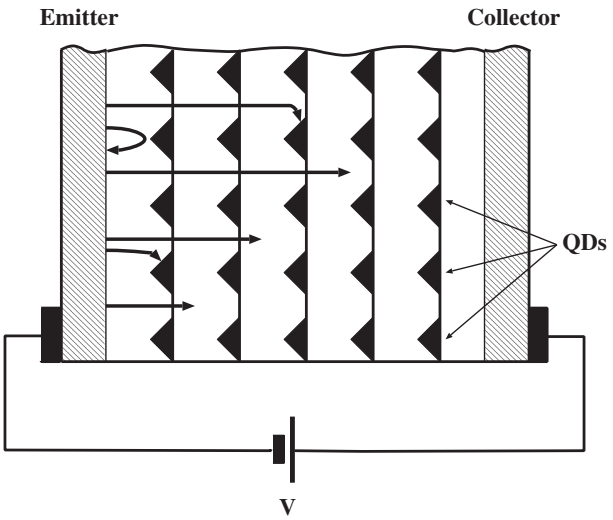

Figure 1. Schematic view of the QDIP structure. Arrows indicate possible trajectories of electrons.

2. The model

We consider a QDIP which constitutes an N^+–N–N^+-diode with a stack of planar arrays of QDs buried in the N-layer. This layer plays the role of the QDIP active region. It is assumed that the QDIP active region is lightly doped by donors. Heavily doped N^+-regions serve as the emitter and collector contacts. The QDIP structure under consideration is shown schematically in figure 1. The current flowing in such a diode under applied voltage is limited by a space charge in the active region. The feature of the current flow in the QDIP diode structure in question is that the space charge is substantially determined by the charges of QDs with the captured electrons. The operation of the QDIP as a photodetector is associated with the photoescape of electrons from QDs due to electron intersubband transitions stimulated by the absorption of infrared photons. The photoexcited electrons contribute to the current and, more importantly, change the space charge in the active region, that leads, in turn, to an increase of the current injected from the emitter contact.

If the numbers of electrons in QDs are sufficiently large, we may assume that these numbers are approximately the same for all QDs in a particular QD array, i.e. $N_k^{i,j} = \langle N_k \rangle$, where i and j are the in-plane indices of QDs and k is the index of the QD array. In this case, the distribution of the electric potential $\varphi = \varphi(x, y, z)$ in the active region is governed by the Poisson equation

$$\left(\frac{\partial^2}{\partial x^2} + \frac{\partial^2}{\partial y^2} + \frac{\partial^2}{\partial x^2}\right)\varphi = \frac{4\pi e}{æ}\left[\sum_{i,j,k}\langle N_k\rangle \delta_\parallel(x - x_i) \times \delta_\parallel(y - y_j)\delta_\perp(z - z_k) - \rho_D\right]. \quad (1)$$

Here, e is the electron charge ($e = |e|$), æ is the dielectric constant, $\delta_\parallel(x)$, $\delta_\parallel(y)$ and $\delta_\perp(z)$ are the QD form-factors in lateral (in the QD array plane) and transverse (growth) directions, respectively, x_i and y_j are the in-plane QD coordinates, $z_k = kL$ is the coordinate of the kth QD array (where $k = 1, 2, 3, \ldots, K$ and K is the number of the QD arrays in the QWIP) and ρ_D is the donor concentration in the active region. The form-factors correspond to the lateral and transverse sizes of QDs equal to a_{QD} and l_{QD}, respectively. The boundary conditions supplementing equation (1) are given by

$$\varphi|_{z=0} = 0, \qquad \varphi|_{z=W} = V, \quad (2)$$

where $W = (K + 1)L$ is the width of the active region and V is the applied voltage.

In the realistic QDIPs, the transverse size of QDs, l_{QD}, is smaller than their lateral size a_{QD} and both of them are smaller than the transverse and lateral spacings between QDs, L and $L_{QD} = \sqrt{\Sigma_{QD}}$, where Σ_{QD} is the density of QDs in each QD array. We shall assume that the QD transverse size is such that the QDs have only one quantum level associated with the electron confinement in the transverse direction, while the lateral size is so large that the total number of quantum levels in QDs and, hence, the maximum number of electrons they can capture $N_{QD} \gg 1$. The electron system in each such a QD can be considered as a degenerate two-dimensional Fermi gas. Similar consideration of many-fermion systems is used in nuclear physics [16].

In equilibrium ($V = 0$), the potential distribution in QDIPs with a moderate doping of the active region exhibits a minimum at the centre of the latter, creating a potential barrier for electrons. This barrier occurs due to the space charge formed by equilibrium electrons occupying QDs (see the appendix). At low voltages ($V < V_0$, where V_0 is the doubled modulus of the potential at its minimum), the systems of electrons in QDs are still close to equilibrium with the contacts, so the space charge is weakly affected by the applied voltage. Thus, in this voltage range, the potential barrier is lowered by the value eVW_m/W and its position, $W_m = W_m(V)$, shifts to the emitter contact when the voltage increases. This gives rise to an increase in the injected current that is very sharp as long as W_m is comparable with W.

In the range of elevated voltages when $eV > eV_0 \gg k_B T$ (where k_B is the Boltzmann constant and T is the temperature), that is more interesting for practical applications, the electron distribution over QDs becomes nonequilibrium. In such a situation, the numbers of electrons in QDs are substantially determined by the current density and the former and the latter should be found self-consistently. The number of electrons occupying a QD of the kth QD array versus the average current density across this array can be obtained using an equation governing the balance of the electron capture into and emission from this QD. Because the electron transport across the active region under the effect of sufficiently strong electric field is associated with the drift, the balance equation can be presented in a form much like that for QWIPs [17, 18]:

$$\frac{\langle j\rangle}{e\Sigma_{QD}} p_k = G_k + \sigma I \langle N_k\rangle. \quad (3)$$

Here, $\langle j\rangle$ is the current density average in lateral directions, p_k is the phenomenological capture parameter (capture probability), G_k is the rate of nonradiative (thermionic or/and tunnelling) emission, σ is the cross section of electron photoescape from QDs and I is the intensity (photon flux) of incident infrared radiation. When the thermionic emission of electrons from QDs dominates the tunnelling emission, one

can use the following formula based on the assumption that electrons in QDs are two dimensional (see, e.g., [14, 18]):

$$G_k = G_0 \exp\left(-\frac{\varepsilon_{\rm QD}}{k_{\rm B}T}\right)\left[\exp\left(\frac{\pi\hbar^2\langle N_k\rangle}{mk_{\rm B}Ta_{\rm QD}^2}\right)-1\right] \simeq G_0 \exp\left[\left(\frac{\pi\hbar^2\langle N_k\rangle}{ma_{\rm QD}^2}-\varepsilon_{\rm QD}\right)\Big/ k_{\rm B}T\right], \quad (4)$$

where G_0 is the pre-exponential factor, $\varepsilon_{\rm QD}$ is the ionization energy of the ground state in QDs, $\hbar$ is the Planck constant and m is the effective mass of electrons in QDs.

The electron capture processes in QDIPs exhibit distinct features [1, 19]. A discrete energy spectrum of electrons in QDs can result in the photon bottleneck effect [20] suppressing the capture of electrons accompanied by the optical phonon emission. This effect can be particularly important in QDIPs with small QDs having a small number of markedly separated bound states. In such QDIPs, the effective suppression of the capture can be also associated with the Pauli exclusion principle when QDs are nearly totally filled with electrons [1]. The electron charges in QDs form potential 'hills' with the tops at the QD centres. These hills are well pronounced in QDIPs with QDs located sufficiently far from each other, i.e. in QDIPs with not too high densities of QDs. The potential hills in question can be rather high, preventing the capture of the electrons propagating in the potential 'valleys' (playing the role of punctures) between QDs [19]. Due to this effect, capture into a QD depends on its potential, which, in turn, is determined by the number of electrons occupying this QD. Indeed, the potential of the QD with indices i, j and k can be estimated as $\varphi_k^{i,j} = -eN_k^{i,j}/C \simeq -e\langle N_k\rangle/C$, where C is the QD geometrical capacitance. Accounting for the effect of limited filling [1] of QDs and the activation character of the electron capture [19] by QDs, the capture parameter as a function of the numbers of electrons in QDs can be taken as being governed by the following equation:

$$p_k = p_0\frac{N_{\rm QD}-\langle N_k\rangle}{N_{\rm QD}}\exp\left(-\frac{e^2\langle N_k\rangle}{Ck_{\rm B}T}\right), \quad (5)$$

where $p_0 \propto N_{\rm QD}\Sigma_{\rm QD}a_{\rm QD}^2$ is the capture parameter for uncharged QDs. As follows from equations (3) and (4), the numbers of electrons occupying the QDs depend on the QD array index k only if the capture parameter is different for the QD arrays with different index. The difference in the capture parameters of different QD arrays can be associated with a nonuniformity of the electric field in the active region, which, in turn, results in a nonuniform heating of electrons. A similar situation occurs in QWIPs with multiple QWs [21, 22], in which the capture rate can be fairly sensitive to the electron heating [23, 24]. However, the electron heating is a nonlocal effect. Hence, the electron capture rate into the QDs of each specific QD array depends on the distribution of the electric field in some area surrounding this QD array (compare with the case of QWIPs [22, 24, 25]). If the energy relaxation length of mobile electrons in the active region is comparable to or longer than the width of this region, the average energy of such electrons and the rate of their capture are determined by the average electric field $E = V/W$. In this situation, the capture parameters of different QD arrays should be the same. Taking this reasoning into account, we (as in some models of QWIPs [18]) put in the following $p_k = p$ and $\langle N_k\rangle = \langle N\rangle$.

When $V > V_0$, the injected current is controlled by a potential barrier formed by a series of the potential hills belonging to the QD array located near the emitter contact. Apart from the charges of electrons occupying the first QD array, the charges of remote QDs and donors participate in the formation of this barrier. The potential barrier height has maxima at QDs and minima between them. These minima form the punctures through which the main part of the injected current flows. To calculate the current one needs to find the height of the potential barrier as a function of the in-plane coordinates using equations (1) with conditions (2). Considering the effect of different charges on the punctures, we discriminate the average contribution of distant QDs and donors and the immediate contribution of the charges of four QDs of the first QD array surrounding each puncture. Thus, the potential of the first QD array can be presented in the form

$$\varphi_1 = \langle\varphi_1\rangle + (\psi - \langle\psi\rangle). \quad (6)$$

Here and below, $\varphi_k = \varphi(x, y, kL)$. Averaging equation (1) in the lateral direction, one can arrive at

$$\frac{{\rm d}^2\langle\varphi\rangle}{{\rm d}z^2} = \frac{4\pi e}{æ}\left[\Sigma_{\rm QD}\langle N\rangle\sum_{k=1}^{K}\delta_\perp(z-kL)-\rho_{\rm D}\right]. \quad (7)$$

A rigorous solution of equation (7) with conditions (2) for QDIPs with arbitrary numbers of the QD arrays can be presented as

$$\langle\varphi_k\rangle = V\frac{k}{(K+1)} + \frac{2\pi eL^2}{æ}\left(\rho_{\rm D}-\langle N\rangle\frac{\Sigma_{\rm QD}}{L}\right)(K+1-k)k. \quad (8)$$

Equation (8) immediately yields

$$\langle\varphi_1\rangle = \frac{V}{(K+1)} + \frac{2\pi eL^2K}{æ}\left(\rho_{\rm D}-\langle N\rangle\frac{\Sigma_{\rm QD}}{L}\right). \quad (9)$$

Considering QDIPs with $a_{\rm QD} \ll L_{\rm QD} = \Sigma_{\rm QD}^{-1/2}$, for ψ near the puncture at the point ($x_i = 0, y_j = 0, z_1 = L$) and for $\langle\psi\rangle$ one obtains

$$\psi = -\frac{e\langle N\rangle}{æ}\left[\frac{1}{\sqrt{(x-L_{\rm QD}/\sqrt{2})^2+y^2}} + \frac{1}{\sqrt{(x+L_{\rm QD}/\sqrt{2})^2+y^2}} + \frac{1}{\sqrt{x^2+(y-L_{\rm QD}/\sqrt{2})^2}} + \frac{1}{\sqrt{x^2+(y+L_{\rm QD}/\sqrt{2})^2}}\right] \simeq -\frac{4\sqrt{2}e\langle N\rangle\sqrt{\Sigma_{\rm QD}}}{æ}\left[1+\frac{1}{2}\Sigma_{\rm QD}(x^2+y^2)\right] \quad (10)$$

and

$$\langle\psi\rangle \simeq -\frac{1}{L_{\rm QD}^2}\int_{-L_{\rm QD}/2}^{L_{\rm QD}/2}\int_{-L_{\rm QD}/2}^{L_{\rm QD}/2}{\rm d}x\,{\rm d}y\,\psi = -\frac{4\sqrt{2}e\langle N\rangle\sqrt{\Sigma_{\rm QD}}}{æ}(1+\xi), \quad (11)$$

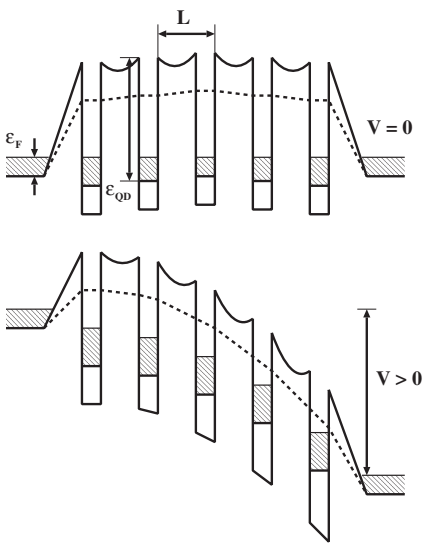

Figure 2. Conduction band edge versus coordinate. Solid and dashed curves correspond to the active region cross sections passing through the centres of QDs and between them, respectively.

where

$$\xi = \frac{1}{\sqrt{2}} \ln \frac{(1+\sqrt{5})(2+\sqrt{5})}{2} - 1 \simeq 0.361.$$

A qualitative view of the cross sections of the conduction band edge profile is shown in figure 2.

The current through each puncture is proportional to $j_m \exp(e\varphi_1/k_BT)$, where j_m is the maximum current density which can be supplied by the emitter contact. Hence, the average current density $\langle j \rangle$ is given by

$$\langle j \rangle \simeq j_m \Sigma_{QD} \int_0^\infty dr^2 \exp\left(\frac{e\varphi_1}{k_BT}\right), \tag{12}$$

where $r^2 = x^2 + y^2$ and the upper limit of integration is extended to infinity.

Using equations (5) and (9)–(12), one can arrive at the following equation relating the average current density $\langle j \rangle$ and the number of electrons in QDs $\langle N \rangle$:

$$\langle j \rangle \simeq j_m \left(\frac{2\Theta}{\langle N \rangle}\right) \exp\left[\frac{\langle N \rangle}{\Theta}\left(\xi - \frac{\pi K}{2\sqrt{2}}\sqrt{\Sigma_{QD}}L\right)\right] \times \exp\left[\frac{e(V+V_D)}{(K+1)k_BT}\right]. \tag{13}$$

Here, the following notations are used:

$$\Theta = \frac{æ k_B T}{4\sqrt{2}e^2\sqrt{\Sigma_{QD}}} \quad \text{and} \quad V_D = \frac{2\pi e \rho_D}{æ} L^2 K(K+1).$$

3. Dark current

In dark conditions ($I = 0$), equations (3)–(5) yield

$$\langle N \rangle \left(1 + \frac{C_{QD}}{C}\right) = N_0 + \frac{m k_B T a_{QD}^2}{\pi\hbar^2} \ln\left[\frac{\langle j \rangle\, p_0 (N_{QD} - \langle N \rangle)}{e G_0 \Sigma_{QD} N_{QD}}\right], \tag{14}$$

where $C_{QD} = me^2 a_{QD}^2/\pi\hbar^2$ is the quantity that can be called the QD quantum capacitance [26], and

$$N_0 = \frac{m a_{QD}^2 \varepsilon_{QD}}{\pi\hbar^2} \simeq \left(\frac{a_{QD}}{l_{QD}}\right)^2,$$

so $N_0 \simeq N_{QD}$. Assuming that QDs have the form of a circular disc ($l_{QD} \ll a_{QD} \ll L$), one can obtain [27] $C \simeq (2æ\, a_{QD}/\pi^{3/2})$ and $C_{QD}/C = \sqrt{\pi} a_{QD}/2a_B$, where $a_B = æ\hbar^2/me^2$ is the Bohr radius.

One may anticipate that at the voltages when the current density is not too large (see below), one has $\langle N \rangle < N_{QD}$. Substituting $\langle N \rangle$, following in this case from equation (14), into (13) and introducing the dimensionless current densities $i = \langle j \rangle p_0/eG_0\Sigma_{QD}$ and $i_m = j_m p_0/eG_0\Sigma_{QD}$, we obtain the following equation:

$$i^\gamma \simeq i_m \left(\frac{2\Theta}{N_0}\right) \exp\left[\left(\frac{e(V+V_D)}{K+1} - (\gamma-1)\varepsilon_{QD}\right) \Big/ k_BT\right] \tag{15}$$

or

$$i \simeq \left(i_m \frac{2\Theta}{N_0}\right)^{\frac{1}{\gamma}} \exp\left[\left(\frac{e(V+V_D)}{(K+1)} - (\gamma-1)\varepsilon_{QD}\right) \Big/ \gamma k_BT\right]. \tag{16}$$

Here,

$$\gamma = 2K\Sigma_{QD} a_{QD}^2 \left(\frac{L}{a_B}\right)\left[\frac{1-\eta}{1+(\sqrt{\pi}a_{QD}/2a_B)}\right] + 1, \tag{17}$$

where $\eta = (2\sqrt{2}\xi/\pi K L\sqrt{\Sigma_{QD}}) \simeq 0.324/KL\sqrt{\Sigma_{QD}}$. In QDIPs with sufficiently large number of QD arrays and high density of QDs in each array, the parameter η is small. This means that the averaged action of the QD and donor charges dominates if $KL\sqrt{\Sigma_{QD}} > 1$. However, in QDIPs with a few QD arrays and relatively low density of QDs (i.e. with large punctures), this parameter can be comparable to unity, resulting in a small value of γ. The latter case corresponds to a very low potential barrier between QDs and, hence, a large current through the punctures.

Estimating γ for QDIPs with $K = 20$, $\Sigma_{QD} = (10^{10}$–$10^{11})$ cm^{-2} and $L = 30$ nm, $a_{QD} = 15$ nm, $a_B = 15$ nm, i.e. similar to QDIPs studied experimentally [6], one can obtain $\gamma \simeq 3$–21. For QDIPs having $K = 3$, $\Sigma_{QD} = (10^{10}$–$10^{11})$ cm^{-2} $L = 40$, $a_{QD} = 15$ nm and $a_B = 15$ nm (as in [10]), one has $\gamma \simeq 1.5$–5. Thus, in realistic QDIPs, parameter γ can be both moderate and fairly large. The value i_m can be large due to high maximum current density that can be provided by a heavily doped emitter contact. Conversely, one has $\Theta/N_0 \leqslant 1$. If γ is sufficiently large in comparison with unity, one may assume that with a good accuracy $(2i_m\Theta/N_0)^{1/\gamma} \simeq 1$. Hence, from equation (16) one can obtain

$$\langle j \rangle \simeq \left(\frac{e\Sigma_{QD}G_0}{p_0}\right) \exp\left[\left(\frac{e(V+V_D)}{(K+1)} - (\gamma-1)\varepsilon_{QD}\right) \Big/ \gamma k_BT\right]. \tag{18}$$

Substituting $\langle j \rangle$ from equation (18) into (14), one can obtain

$$\langle N \rangle \simeq \frac{N_{QD}}{V_{QD}}\left[V + V_D + (K+1)\frac{\varepsilon_{QD}}{e}\right], \tag{19}$$

where $V_{QD} = 2\pi eK(K+1)\Sigma_{QD}L(1-\eta)N_{QD}/æ$. As can be seen from equation (18), the number of electrons occupying QDs increases with increasing voltage and formula (18) for the dark current derived above is valid when $\langle N\rangle < N_{QD}$. Invoking equation (19) and assuming for simplicity that $V_{QD} \gg (K+1)\varepsilon_{QD}/e$, one can arrive at the following limitation:

$$V_0 < V \ll (V_{QD} - V_D) = \frac{2\pi eK(K+1)L^2}{æ} \times \left(N_{QD}\frac{\Sigma_{QD}}{L} - \rho_D\right). \quad (20)$$

For a QDIP with a large number of QD arrays and a high QD density, for example, for $K = 20$, $L = 30$ nm and $\Sigma_{QD} = 10^{11}$ cm^{-2}, one obtains $(V_{QD} - V_D) \simeq 90 \times (N_{QD} - N_D)$ V. Here, the number of donors per QD, $N_D = \rho_D L/\Sigma_{QD}$, is introduced. Taking into account that V_0 is about a few tenths of a volt (see the appendix), this estimate implies that the voltage range in which QDs are not totally filled and, hence, the range of validity of the formulae for the dark current obtained above can be very wide (except the case when the number of donors per QD is close to the maximum number of electrons captured by each QD). However, for a QDIP, say, with $K = 5$, $L = 30$ nm and $\Sigma_{QD} = 10^{10}$ cm^{-2}, the estimate yields $(V_{QD} - V_D) \simeq 0.56 \times (N_{QD} - N_D)$ V. In the latter case, the validity of equation (18) is questionable.

When V becomes comparable to $(V_{QD} - V_D)$, all QDs in the QDIP active region can be strongly filled ($\langle N\rangle \simeq N_{QD}$). In such a situation, simultaneous solution of equations (13) and (14) results in the following formula:

$$\langle j\rangle \simeq j_m\left(\frac{2\Theta}{N_{QD}}\right)\exp\left[\frac{e(V + V_D - V_{QD})}{(K+1)k_BT}\right]. \quad (21)$$

Due to the smallness of quantity Θ/N_{QD}, up to the voltages $V \leqslant (V_{QD} - V_D)$, one has $\langle j\rangle \ll j_m$. One can see from equation (21) that in the case under consideration the dark-current–voltage characteristic is determined by lowering of the potential barrier by the value $eV/(K+1)$ (compare with [1]), which is larger than in the case when QDs are filled with electrons only partially. Due to this, the dark-current–voltage characteristic (21) is steeper than that given by equation (18). The point is that in the situation when QDs are not filled totally and, consequently, are able to capture additional electrons, the further accumulation of electrons with increasing voltage prevents a steep decrease in the potential height.

At higher voltages $V > (V_{QD} - V_D)$, the electron space charge accumulated in QDs becomes fixed. In such a regime, which is certainly not interesting for the application of QDIPs as photodetectors, the dark current in QDIPs becomes limited by the space charge of the injected mobile electrons, eventually tending to the saturation value j_m.

4. Analysis

Considering the behaviour of the potential barrier in the QDIP active region in the states when the numbers of electrons in QDs are close to their equilibrium values, one can find that in the range of very low voltages (when $eV < k_BT$)

$$\langle j\rangle \propto \frac{eV}{k_BT}. \quad (22)$$

When $k_BT \ll V \leqslant V_0$, the dark-current density increases exponentially with the characteristic voltage about V_0.

At elevated voltages $V > V_0$, as can be seen from equation (18), the shape of the dark-current–voltage characteristic strongly depends on the parameter γ. In QDIPs with a large parameter γ, the dark current practically does not depend on j_m, i.e. on the emitter contact parameters such as j_m. Equation (18) yields a steep (exponential) dark-current–voltage characteristic, so that

$$\ln\langle j\rangle \propto \frac{V}{V_1}, \quad (23)$$

where the characteristic voltage is given by

$$V_1 = (K+1)\gamma\left(\frac{k_BT}{e}\right), \quad (24)$$

when $V_0 < V \ll (V_{QD} - V_D)$, and

$$V_1 = (K+1)\left(\frac{k_BT}{e}\right), \quad (25)$$

when $V_0 \ll V \leqslant (V_{QD} - V_D)$.

The electric-field dependence of the QD ionization energy can also affect the dark-current–voltage characteristic, making it slightly steeper. In the simplest approach, setting $\varepsilon_{QD} = \varepsilon^0_{QD} - [el_{QD}V/2(K+1)L]$, one can find that quantity V_1^{-1} in equation (23) should be substituted for $(V_1 + V_2)/V_1V_2$, where $V_2 \simeq 2K(\frac{L}{l_{QD}})(\frac{k_BT}{e})$. The ratio of these characteristic voltages is equal to

$$\frac{V_1}{V_2} = \frac{K\Sigma_{QD}a^2_{QD}(1-\eta)}{1 + (\sqrt{\pi}a_{QD}/2a_B)}\left(\frac{l_{QD}}{a_B}\right).$$

In QDIPs with not too large K and Σ_{QD}, one has $V_1/V_2 < 1$.

The characteristic voltage V_1 that determines the steepness of the QDIP dark-current–voltage characteristic depends on many structural parameters. According to equations (24), for a QDIP with $K = 10$, $\Sigma_{QD} = 1.4 \times 10^{10}$ cm^{-2}, $L = 100$ nm, $a_{QD} = 15$ nm and $a_B = 15$ nm at $T = 40$ K, $V_1 \simeq 0.1$ V. The theoretical dark-current–voltage characteristics calculated for these parameters in some range of the QD densities and the experimental one [8] are shown in figure 3, demonstrating excellent agreement over three orders of magnitude. For a QDIP with $K = 20$ and $L = 30$ nm (similar to those studied experimentally in [6]), assuming that $a_{QD} = 15$ nm, $a_B = 15$ nm and $\Sigma_{QD} = 10^{10}$ cm^{-2}, we obtain $eV_1/k_BT \simeq 35$. The experimental data extracted from [6] in the temperature range $T = 60$–100 K correspond to $eV_1/k_BT \simeq 30$–31.

Equation (18) with equation (24) describe the following dependence of the dark current versus the density of QDs at not too high voltages:

$$\ln\langle j\rangle \propto \frac{1}{K(K+1)\Sigma_{QD}}. \quad (26)$$

Figure 4 shows the dark current as a function of relative density of QDs $\Sigma_{QD}a^2_{QD}$ at different applied voltages calculated using equation (18).

Equations (18) and (21) explicitly show that the dark current strongly increases with increasing doping level of the

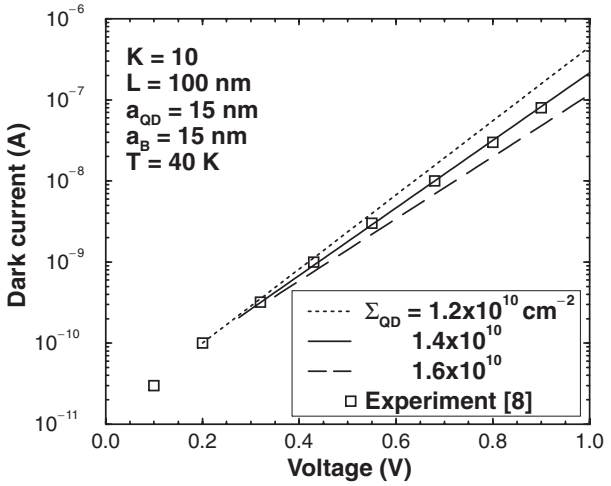

Figure 3. Calculated and experimental dark-current–voltage characteristics.

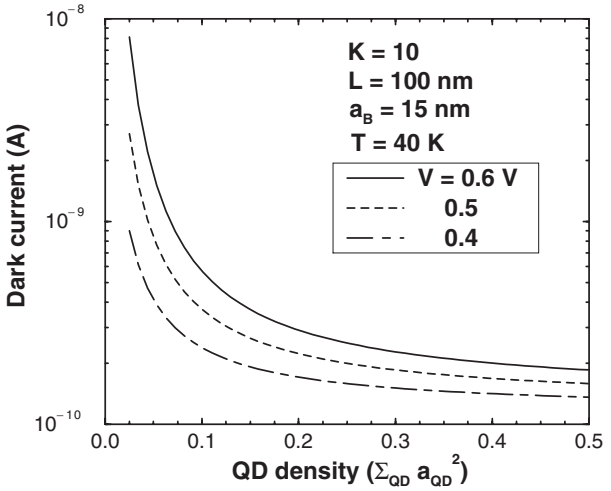

Figure 4. Dark current versus relative QD density $\Sigma_{\rm QD}a_{\rm QD}^2$ at different voltages.

QDIP active region. Indeed, from equations (18) and (21), for the ratio of the dark current in QDIPs with doped ($\langle j\rangle$) and undoped ($\langle j_0\rangle$) active regions one can obtain (when $a_{\rm QD} \simeq a_{\rm B}$)

$$\ln \frac{\langle j\rangle}{\langle j_0\rangle} \propto \rho_{\rm D}. \tag{27}$$

For QDIPs with donors placed directly in the QD array planes, in all the above formulae one should substitute $\rho_{\rm D}$ for $\Sigma_{\rm D}/L$, where $\Sigma_{\rm D}$ is the sheet donor concentration in each QD array.

In our calculations we did not discriminate the effective temperatures of electrons in the contacts, QDs and punctures. However, the electrons propagating through the punctures can be markedly heated if the average electric field across the QDIP active region is sufficiently strong. The electron heating can affect the capture processes and, consequently, the QDIP characteristics. To include this effect, one can replace the lattice temperature T in equation (5) by an effective temperature $T_{\rm eff}$. This results in the renormalization of the parameter γ, which, in such a case, is given by

$$\gamma \simeq \frac{2K\,\Sigma_{\rm QD}a_{\rm QD}^2(L/a_{\rm B})(1-\eta)}{[1+(\sqrt{\pi}a_{\rm QD}/2a_{\rm B})(T/T_{\rm eff})]} + 1. \tag{28}$$

According to equation (28), the transition from $T_{\rm eff} = T$ to $T_{\rm eff} > T$ can result in a twofold increase in γ and, consequently, in V_1.

5. Comparison of QDIPs and QWIPs

The direct comparison of QDIPs and QWIPs is complicated by distinctions between the injection mechanisms in QDIPs under consideration and those studied experimentally and QWIPs, in most of which the injection is of tunnelling origin (except [15, 28], where fabrication and testing of QWIPs with thermionic injection were reported). Because of this, we shall compare the QDIP characteristics obtained above and the characteristics of QWIPs with thermionic injection calculated in [29], bearing in mind that such QWIPs do not always exhibit the best performace. Roughly estimating the ratio of the dark currents in QDIPs and QWIPs with thermionic injection, we leave aside, for simplicity, the effect of electron heating. The calculation of the dark-current density in QWIPs with a large number of QWs and thermionic injection of electrons from the emitter contact (such QWIPs with a single QW were studied theoretically in [14]) results in the following formulae [29]:

$$\langle j_{\rm QW}\rangle = \left(\frac{eg_0}{p_{\rm QW}}\right)\left(\frac{j_{\rm m}p_{\rm QW}}{eg_0}\right)^{\frac{1}{\gamma_{\rm QW}}} \times \exp\left[\left(\frac{e(V+V_{\rm D})}{(K+1)} - (\gamma_{\rm QW}-1)\varepsilon_{\rm QW}\right)\Big/\gamma_{\rm QW}k_{\rm B}T\right]. \tag{29}$$

Here,

$$\gamma_{\rm QW} = 2K\left(\frac{L}{a_{\rm B}}\right) + 1, \tag{30}$$

g_0 is the characteristic rate of the electron thermionic emission from a QW per unit of its area, $p_{\rm QW}$ is the capture parameter and $\varepsilon_{\rm QW}$ is the QW ionization energy. Comparing γ and $\gamma_{\rm QD}$ by application of equations (17) and (30), one can see that $\gamma < \gamma_{\rm QW}$. This is mainly owing to the smallness of $\Sigma_{\rm QD}a_{\rm QD}^2$. The relative smallness of parameter γ is associated also with factors $(1-\eta)$ and $[1+(\sqrt{\pi}a_{\rm QD}/2a_{\rm B})]^{-1}$, arising due to the lowering of the potential barrier in the punctures with increasing density of QDs and the exponential decrease in the capture rate when the number of electrons in QDs increases.

Consider $\gamma_{\rm QW} \gg 1$ equation (29) can be simplified and reduced to the following:

$$\langle j_{\rm QW}\rangle \simeq \left(\frac{eg_0}{p_{\rm QW}}\right)\exp\left[\left(\frac{e(V+V_{\rm D})}{(K+1)} - (\gamma_{\rm QW}-1)\varepsilon_{\rm QW}\right)\Big/\gamma_{\rm QW}k_{\rm B}T\right]. \tag{31}$$

Using equations (18) and (30), for QDIPs and QWIPs with equal doping levels and ionization energies and γ, $\gamma_{\rm QD} \gg 1$, we find

$$\frac{\langle j\rangle}{\langle j_{\rm QW}\rangle} \simeq \left(\frac{\Sigma_{\rm QD}G_0}{g_0}\right)\left(\frac{p_{\rm QW}}{p_0}\right) \times \exp\left[\frac{e(V+V_{\rm D})}{(K+1)k_{\rm B}T}\left(\frac{1}{\gamma} - \frac{1}{\gamma_{\rm QW}}\right)\right]. \tag{32}$$

Taking γ and γ_{QD} from formulae (17) and (30), respectively, and employing equation (32), one can obtain

$$\ln\frac{\langle j\rangle}{\langle j_{QW}\rangle} \simeq \ln\frac{p_{QW}}{p_0} + \left(\frac{V+V_D}{V_1}\right) \times\left[1-\frac{\Sigma_{QD}a_{QD}^2(1-\eta)}{1+(\sqrt{\pi}a_{QD}/2a_B)}\right] \simeq \left(\frac{V+V_D}{V_1}\right). \quad (33)$$

As follows from equation (33), if p_{QW} and p_0 are of the same order of magnitude, the dark current in QDIPs with $\Sigma_{QD}a_{QD}^2 \ll 1$ is markedly higher than that in QWIPs. One needs therefore to recall that p_0 can be much larger than p given by formula (5).

The QDIP dark-current–voltage characteristics are pronouncedly steeper than those for a QWIP. This conclusion is confirmed by the comparison of the experimental dark-current–voltage characteristics of QDIPs [6, 8] and QWIPs [15].

6. Conclusions

In summary, we have proposed a device model for realistic QDIPs in dark conditions. This model self-consistently accounts for (a) the effect of the electron charges captured in QDs and the donor charges on the spatial distribution of the electric potential in the QDIP active region, (b) the activation character of the electron capture and the limitation of the capture rate due the Pauli principle, (c) the thermionic electron emission from QDs and thermionic injection of electrons from the emitter contact into the QDIP active region and (d) the existence of the punctures between QDs through which the main portion of the injected current flows. Using the developed model, we have derived the average dark current density as a function of the QDIP structural parameters, applied voltage and temperature in explicit analytical form. The obtained results explain a rather sharp dark-current–voltage characteristic of QDIPs and strong dependence of the dark current on the density of QDs in the QD arrays and the doping level of the active region observed in experiments. The calculated characteristics of QDIPs are in good agreement with those obtained experimentally. We have also carried out a comparison of the characteristics of QDIPs and QWIPs having similar parameters.

Acknowledgments

The authors are thankful to N Tsutsui for assistance in calculations and technical help. The work at WSU was supported by the US Army Research Office.

Appendix

In equilibrium when there is no applied voltage, considering that the electron systems in QDs are two dimensional and degenerate, and that their Fermi level coincides with the Fermi level of the electron gas in the contacts, we have

$$\langle N_k\rangle = \frac{ma_{QD}^2}{\pi\hbar^2}[e\langle\varphi(kL)\rangle + \varepsilon_{QD} - \varepsilon_F], \quad (A.1)$$

where ε_{QD} and ε_F are the QD ionization energy and the Fermi energy of electrons in the contacts counted from the edge of the conduction band in the latter. Substituting $\langle N_k\rangle$ from equation (A.1) into (3), we arrive at

$$\frac{d^2\langle\varphi\rangle}{dz^2} = \frac{4\Sigma_{QD}a_{QD}^2}{a_B L}(\langle\varphi\rangle + \varphi_{QD}), \quad (A.2)$$

where $\varphi_{QD} = \varepsilon_{QD}/e - \varepsilon_F(\pi e\rho_D/æ)(a_B L/\Sigma_{QD}a_{QD}^2)$. Normally, i.e. at not too high doping levels of the contacts and the active region, $\varphi_{QD} > 0$. In the case $K \gg 1$, solving equation (A.2) with boundary conditions (2) for $V = 0$, we obtain

$$\langle\varphi_k\rangle = \varphi_{QD}\left[\frac{\cosh(2kL-W)/L_S}{\cosh(W/L_S)} - 1\right], \quad (A.3)$$

where $L_S = \sqrt{a_B L/\Sigma_{QD}a_{QD}^2}$. The averaged potential has a minimum at $z = W_m = W/2$, where $\langle\varphi\rangle = \langle\varphi_m\rangle$. Using equations (A.1) and (A.3), one can obtain the following expression for $\langle\varphi_m\rangle$:

$$\langle\varphi_m\rangle = \varphi_{QD}\left[\frac{1}{\cosh(W/L_S)} - 1\right]. \quad (A.4)$$

When $V > 0$, the minimum shifts to the contact. The voltage at which the minimum shifts from the centre of the QDIP active region to the first array of QD can be estimated as $V_0 \simeq -2\langle\varphi_m\rangle$. Choosing K = 10–20, ε_{QD} = 150–200 meV, $\Sigma_{QD} = (10^{10}$–$10^{11})$ cm^{-2}, L = 30 nm, a_{QD} = 15 nm and a_B = 15 nm and neglecting doping one can find $V_0 \simeq$ 0.2–0.4 V.

References

[1] Ryzhii V 1996 *Semicond. Sci. Technol.* **11** 759
[2] Phillips J, Kamath K and Bhattacharya P 1998 *Appl. Phys. Lett.* **72** 2020
[3] Kim S, Mohseni H, Erdtmann M, Michel M, Jelen J and Razeghi M 1998 *Appl. Phys. Lett.* **73** 963
[4] Pan D, Towe E and Kennerly S 1998 *Appl. Phys. Lett.* **73** 1937
[5] Maimon S, Finkman E, Bahir G, Schacham S E, Garcia J M and Petroff P M 1998 *Appl. Phys. Lett.* **73** 2003
[6] Xu S J *et al* 1998 *Appl. Phys. Lett.* **73** 3153
[7] Horiguchi N, Futatsugi T, Nakata Y, Yokoyama N, Mankad T and Petroff P M 1999 *Japan. J. Appl. Phys.* **38** 2559
[8] Phillips J, Bhattacharya P, Kennerly S W, Beekman D W and Dutta M 1999 *IEEE J. Quantum Electron.* **35** 936
[9] Pan D, Towe E and Kennerly S 1999 *Appl. Phys. Lett.* **75** 2719
[10] Chu L, Zrenner A, Böhm G and Abstreiter G 1999 *Appl. Phys. Lett.* **75** 3599
[11] Levine B F 1992 *J. Appl. Phys.* **74** R1
[12] Gunapala S D and Bandara S V 2000 *Intersubband Transitions in Quantum Wells: Physics and Device Application* vol 1, ed H C Liu and F Capasso (San Diego: Academic) p 197
[13] Helm M 2000 *Intersubband Transitions in Quantum Wells: Physics and Device Application* vol 1, ed H C Liu and F Capasso (San Diego: Academic) p 1
[14] Ryzhii V and Ershov M 1995 *J. Appl. Phys.* **78** 1214
[15] Perera A G U, Matsik S G, Liu H C, Gao M, Buchanan M, Schlaff W J and Yeo W 2000 *Appl. Phys. Lett.* **77** 741
[16] Ring P and Schuck P 1980 *The Nuclear Many-Body Problem* (New York: Springer)
[17] Liu H C 1992 *Appl. Phys. Lett.* **60** 1507
[18] Ryzhii V 1997 *J. Appl. Phys.* **81** 6442

[19] Mitin V V, Pipa V I, Sergeev A V, Dutta M and Stroscio M 2000 *24th Workshop on Compound Semicond. Devices and Integrated Circuits (Augen Sea)* abstracts pp XIY–15
[20] Bockelmann U and Bastard G 1990 *Phys. Rev.* B **42** 8947
[21] Ryzhii V and Liu H C 1999 *Japan. J. Appl. Phys.* **38** 5815
[22] Ryzhii M and Ryzhii V 1999 *Japan. J. Appl. Phys.* **38** 5922
[23] Ryzhii M, Ryzhii V and Willander M 1999 *Japan. J. Appl. Phys.* **38** 6650
[24] Ryzhii M, Ryzhii V, Suris R and Hamaguchi C 2000 *Phys. Rev.* B **61** 2742
[25] Ryzhii V, Khmyrova I, Ryzhii M, Suris R and Hamaguchi C 2000 *Phys. Rev.* B **62** 7268
[26] Luryi S 1988 *Appl. Phys. Lett.* **52** 501
[27] Landau L D and Lifshitz E M 1984 *Electrodynamics of Continuous Media* (Oxford: Pergamon)
[28] Gunapala S D, Bandara K M S V, Levine B F, Sarusi G, Sivco D L and Cho A Y 1994 *Appl. Phys. Lett.* **64** 2288
[29] Ryzhii V 2000 unpublished